Appendix: Evaluation of a Fast-Solving Rigid Body Spine Model Inclusive of Intra-Abdominal Pressure

Siril Teja Dukkipati and Mark Driscoll

I. Appendix

This appendix describes the models provided in the Github repository, instructions to simulate the models and other interesting data that could not be included in the original manuscript.

A. Model Repository

The repository can be accessed at: https://github.com/siril-teja/RBDmodel-io.git. It contains the main project file named *RBDmodel-io.prj* which can be opened in MATLAB. Note that Simulink 2023a or a newer version is required to run this model. To run any optimization, Simulink Design Optimization or Control System Toolbox is needed.

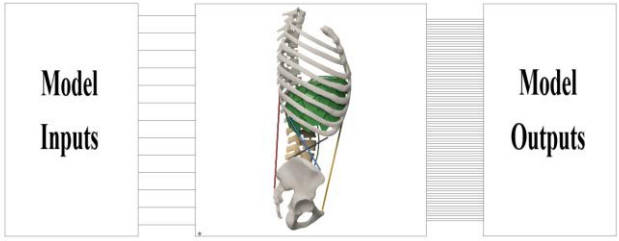

Fig. 1. Schematic of the MATLAB Simulink model

The Simulink model contains three main blocks. The model input and output blocks are editable and are used to pass arguments and fetch responses to and from the main model. The user can add more inputs and derive new output measurements by editing these blocks accordingly. The main model is not editable in the current version.

1) Model Inputs

Model inputs facilitate simulating the model in different loading scenarios. They can either be a constant value or a time varying signal. All the tunable inputs of the model are listed below.

TABLE I

Parameter	Description
IAP_Pa	Intra-abdominal pressure in Pascals, used in IAP Model 1.
Left_RA *Right_RA*	Left and right rectus abdominus muscle force in Newtons.
Left_MF *Right_MF*	Left and right rectus multifidus force in Newtons.
Left_IO *Right_IO*	Left and right internal oblique muscle force in Newtons.
Left_EO *Right_EO*	Left and right external oblique force in Newtons.
Moment_FE	Flexion-extension (FE) moment at L1 in Nm.
Moment_LB	Lateral bending moment (LB) at L1 in Nm.
Moment_AR	Axial rotation (AR) moment at L1 in Nm.

Table 1. Tunable parameters in the RBD model.

The pelvis of the model is fixed in all degrees of freedom relative to the ground. Since the main model is protected, some input parameters that were discussed in the original manuscript needed to be fixed. These parameters were directly referenced inside the Simulink blocks and could not be tuned from outside the main model. They are listed below.

TABLE II

Parameter	Description
C_Gimbal	This is the damping coefficient used in all the IVD 3DoF gimbal joints. This is set to 0.1Nm/(deg/sec), as described in the original manuscript.
K_Gimbal	This is the built-in spring stiffness for all the IVD 3DoF gimbal joints. Since the model uses a custom equation based torque feedback, this parameter is set to 0 N/m.

C_IAP	This is the damping coefficient of the spring damper element used in IAP Model 2. This is set to 0.01 N/(m/s).
K_IAP	This is the spring stiffness of the spring-damper element used in IAP model 2 set to 0 N/m. Refer to Fig. 10 in the manuscript.
a	Scaling factor α used in equation 1, applicable in FE and LB. This is set to 1.
b	Scaling factor α used in equation 1, applicable in AR. This is set to 0.7.
muscle_color	Graphics parameter – not applicable
muscle_radius	Graphics parameter – not applicable

Table 2. Fixed parameters in the RBD model.

2) Model Outputs

An extensive list of model measurements was made available by default. Some of them are:

- L1-S1 moment and range of motion
- Trunk range of motion
- Segmental moments and range of motions
- All ligamentous forces over time
- Sagittal plane kinematics
- Extensor torque profiles due to IAP

In addition to these, the user can create new outputs as desired using the signal lines provided.

3) Optimization

In addition to performing any static simulations, the user has an ability to perform optimization using the tunable parameters as inputs and model outputs as targets. Simulink Design Optimization or Control Systems toolbox is needed for this. Once installed, the user can utilize the "Check Custom Bounds" blocks to model their constraints. Then, the inbuilt Response Optimizer app can be used to define optimization inputs and optimizer settings.

As an example, this video shows the model catching a mass of 1kg from an initial height of 30cm. In this example, the clavicle and scapula were fixed to the ribcage while the humerus and the scapula were constrained using a 1DOF revolute joint with a torsional spring constant of 10Nm/deg. First, all the muscles were turned off and the simulation was run. Then, all the muscle forces were activated, and the optimization algorithm (Fig. 3 in manuscript) was run to find a set of optimized muscle forces that would result in a "stable" spinal pose while the model is catching the cube. Mechanical stability of the spine in this scenario is defined as follows [1]:

"The spine is said to be stable when the plumbline (gravity line) drawn from the center of C7-T1 intervertebral disc falls within ±2cm from the posterior superior aspect of the S1 vertebra."

The palm of the hand and the 1kg mass were connected using stiff springs in x, y, z directions to model momentum transfer between bodies. While the example shown below is simplistic, the model schematic can be used to simulate complex types of loading, like variable gravity (astronauts taking off in a rocket), variable acceleration (crash simulations), etc.

B. Additional Methods

1) IAP Model 1 - Formulation

In this model, the IAP is modeled as a set of discrete normal forces on the diaphragm and the lumbar spine according to the following equation:

$$F_n^{norm} = P_{abd} A_n$$

where F_n^{norm} is the normal force on the n^{th} surface, P_{abd} is the IAP and A_n is the area of the n^{th} surface. To calculate the resultant force on each lumbar vertebra, the effective cross-sectional area of each vertebral body was considered as A_n. This effective area is essentially the cross-sectional area of the vertebral body sectioned by a coronal plane passing through its centroid and normal to the resultant force F_n^{norm}.

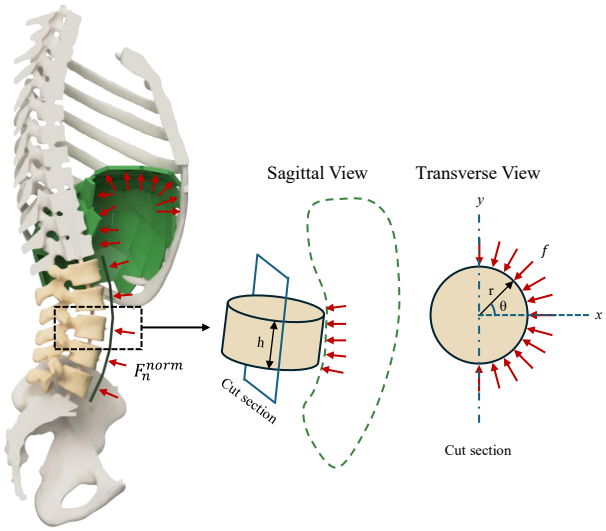

Fig. 2. IAP model 1: Schematic of the resultant force on the lumbar spinal column as a result of IAP.

Let us assume that the vertebral bodies are idealized as cylinders with height h along the Z axis, radius r, and the discrete force vectors represented by $\vec{f}$. This differential force can be written as

$$\begin{aligned} \vec{f} &= -P_{abd}\, \vec{r}\, dA \\ &= -P_{abd}\, \vec{r}\, d\theta\, dz \\ &= -P_{abd}\, r\, (cos\theta\, \vec{x} + sin\theta\, \vec{y})\, d\theta\, dz \end{aligned}$$

Then the resultant force F_n^{norm} is the summation of all these discrete force vectors and can be written as

$$F_n^{norm} = -P_{abd}\, r \int_0^h \int_{\frac{-\pi}{2}}^{\frac{\pi}{2}} (cos\theta\, \vec{x} + sin\theta\, \vec{y})\, d\theta\, dz$$

$$= -P_{abd}\, r\, h \int_{\frac{-\pi}{2}}^{\frac{\pi}{2}} (cos\theta\, \vec{x} + sin\theta\, \vec{y})\, d\theta$$

$$= -P_{abd}\, 2\, r\, h\, \vec{x}$$

i.e. the effective cross-sectional area is

$$A_n = 2\, r\, h$$

C. Additional Results

1) Coupling moments of the spine

It is well documented in literature that the segmental rotations of the spine are coupled. [2], [3], [4], [5], [6]. This was also evidenced in the current model. The tables below describe the level-by-level coupling moments for all three loading directions.

- With a 7.5Nm FE load, no significant lateral bending or axial rotation moments were observed.

TABLE III

Level	Coupled LB load (Nm)	Coupled AR load (Nm)
L1-L2	2.1e-4	2.3e-4
L2-L3	1.2e-4	3.6e-4
L3-L4	1.9e-3	1.2e-3
L4-L5	6.5e-5	2.1e-4
L5-S1	1.4e-3	2.1e-3

Table 3. Coupling when loaded in FE direction

- With a 7.5Nm LB load at L1, the model recorded an average residual axial bending moment of 2.06Nm. No significant flexion moments were observed.

TABLE IV

Level	Coupled AR load (Nm)	Coupled FE load (Nm)
L1-L2	1.82	0.10
L2-L3	0.08	0.10
L3-L4	1.66	0.12
L4-L5	2.76	0.07
L5-S1	3.95	0.32

Table 4. Coupling when loaded in LB direction

- When a 7.5Nm axial bending load at L1 was applied, the model recorded an average lateral bending moment of 1.95Nm. An average flexion-extension moment of 0.65Nm was also observed.

TABLE V

Level	Coupled LB load (Nm)	Coupled FE load (Nm)
L1-L2	1.64	0.90
L2-L3	0.18	0.81
L3-L4	1.60	0.99
L4-L5	2.69	0.40
L5-S1	3.64	0.16

Table 5. Coupling when loaded in AR direction

2) Ligament properties

A bi-linear force-displacement constitutive relation was used to model all the three included ligaments. As an example, the model was loaded in flexion up to a 7.5Nm using a sine wave and the corresponding tensile force developed in the supraspinous ligament was visualized.

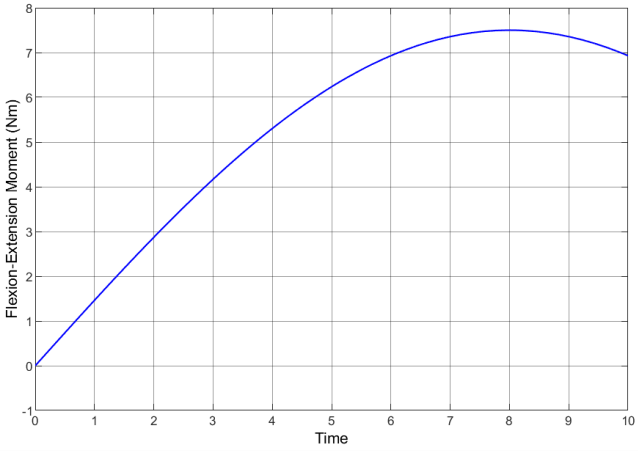

Fig. 3. Applied flexion moment at L1 in Nm with time

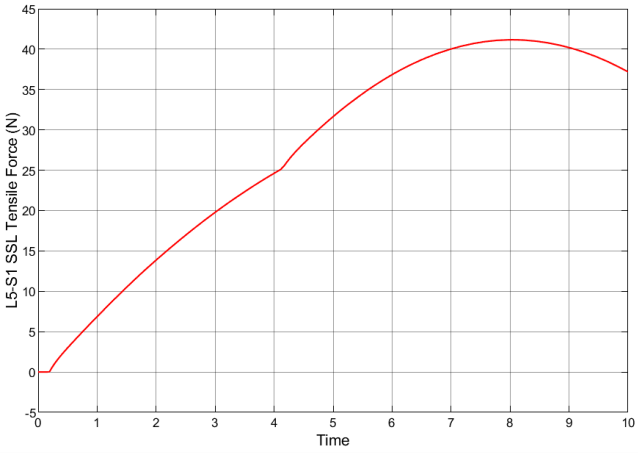

Fig. 4. Resultant tensile force developed in the supraspinous ligament at L5-S1 level

Further, the model outputs block in the included Simulink model can be used to measure ligamentous forces at all the levels for any input load.

3) IVD damping

The 3DoF IVD joints have a damping coefficient parameter set to 0.1 Nm/(deg/sec) by default. Including this parameter in the IVD joint stiffness relationship allows us to capture the hysteresis behavior of the spine, which is a well-documented biomechanical phenomenon. Incorporating damping enhances the physiological realism of the model and aligns it more closely with experimental observations of spinal behavior under

dynamic loading conditions. As the damping constant "c" increases, the hysteresis in the model also increases. This is particularly useful to tune the model to match a different *ex vivo* spine moment-rotation dataset. In practice, it was used to tune the model to match the hysteresis of the 3D printed spine phantom we developed in the past [7], [8].

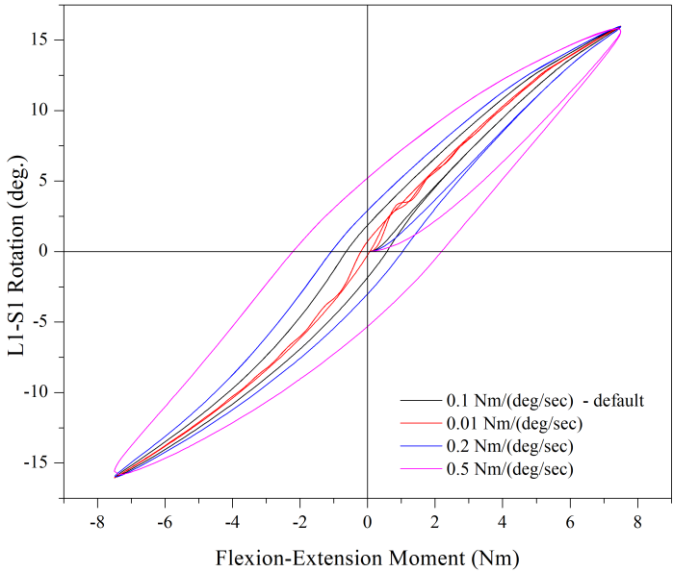

Fig. 5. Model hysteresis variation with IVD joint damping coefficient

4) IAP Model 1 – Extensor torques

The validation of IAP Model 1 was done by comparing the increase in extensor torque at L3 in 50° flexion pose with increase in IAP to *in vivo* study conducted by Hodges et al [9]. It was also compared to a biomechanical model, similar to the current model, presented by Daggfeldt et al [10].

As the *in vivo* comparator data for these complex ethics-bound experiments is limited, validation was carried out at only one lumbar level. Fig. 5 shows the variation of the extensor torque at all lumbar levels to facilitate future model comparisons.

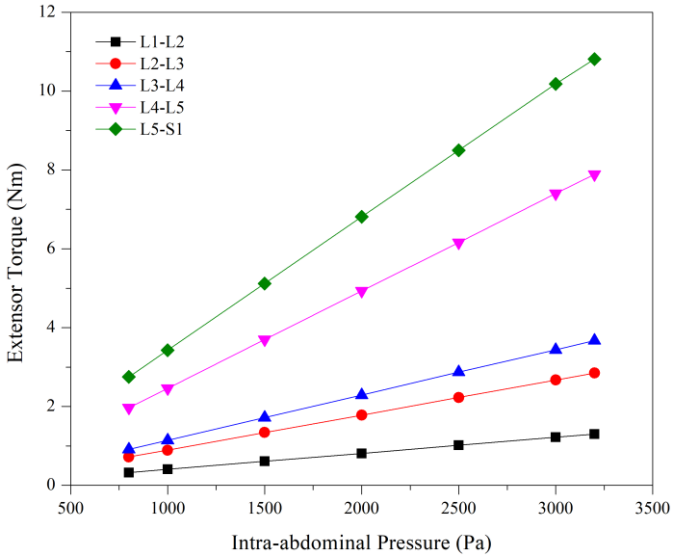

Fig. 6. Extensor torque variation with increase in IAP at all lumbar levels

5) IAP Model 2 – Range of Motion

Validation of IAP Model 2 could not be possible, given the nature of the model. Although the original manuscript contains L1-S1 ROM variation with increase in the abdominal spring constant, the segmental ROMs are given below to facilitate comparison with future models.

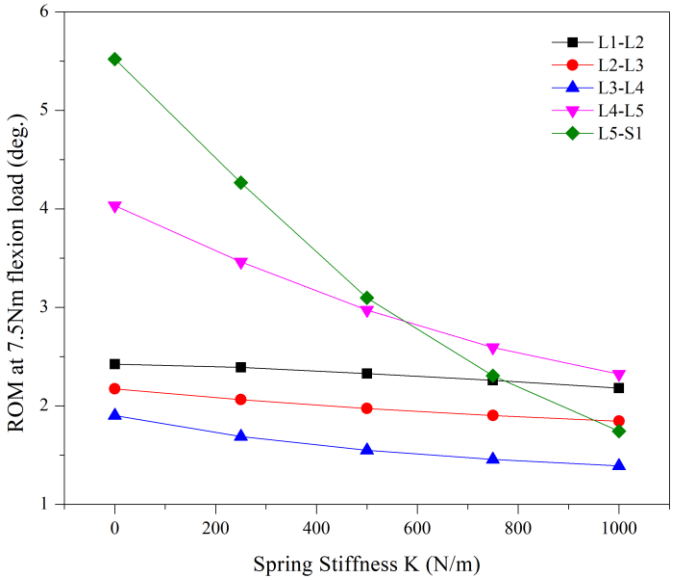

Fig. 7. Segmental range of motion variation with increase in spring stiffness

6) Model Benchmarking

To compare the computational demand of the model in all cases, a benchmarking script (`benchmarking.m`) was included in the repository. This script loads the model, sets the model parameters if any, depending on the case, and simulates the model.

a) Benchmark #1

Per this code, for the following boundary conditions,

- 7.5Nm sinusoidal load at 1 rad/sec external moment at L1 centroid
- Fixed pelvis
- All model components included
- Simulated for 10 seconds

the model compiled in **1.13 seconds**, and run time was **1.7 seconds** (average of n=5 runs).

b) Benchmark #2

To compare the model with Rupp et al. 2015 study [11], the following boundary conditions were imposed:

- Trunk flexion of 50 degrees (90Nm flexion moment at L1)
- Fixed pelvis
- All model components included
- Simulated for 1 sec

The model compiled in **1.18 seconds** and run time was **1.52 seconds.** Rupp et al. reported a run time range of **0.86-0.95 seconds** for their models which are slightly efficient compared

to our model. It is to be noted that these numbers heavily depend on the specifications of the computer the models run on and may differ accordingly. For reference, the presented model was built and simulated on a Windows 11 laptop, with Intel 12th gen i7 processor, and 16 GB of memory.

REFERENCES

[1] R. Q. Knight *et al.*, "White Paper on Sagittal Plane Alignment Terminology," 2010.

[2] A. A. WHITE and M. M. PANJABI, "The Basic Kinematics of the Human Spine," *Spine (Phila Pa 1976)*, vol. 3, no. 1, pp. 12–20, Mar. 1978, doi: 10.1097/00007632-197803000-00003.

[3] M. J. PEARCY and S. B. TIBREWAL, "Axial Rotation and Lateral Bending in the Normal Lumbar Spine Measured by Three-Dimensional Radiography," *Spine (Phila Pa 1976)*, vol. 9, no. 6, pp. 582–587, Sep. 1984, doi: 10.1097/00007632-198409000-00008.

[4] R. S. Ochia *et al.*, "Three-Dimensional In Vivo Measurement of Lumbar Spine Segmental Motion," *Spine (Phila Pa 1976)*, vol. 31, no. 18, pp. 2073–2078, Aug. 2006, doi: 10.1097/01.brs.0000231435.55842.9e.

[5] R. Fujii *et al.*, "Kinematics of the lumbar spine in trunk rotation: in vivo three-dimensional analysis using magnetic resonance imaging," *European Spine Journal*, vol. 16, no. 11, pp. 1867–1874, Nov. 2007, doi: 10.1007/s00586-007-0373-3.

[6] G. Li *et al.*, "Segmental in vivo vertebral motion during functional human lumbar spine activities," *European Spine Journal*, vol. 18, no. 7, pp. 1013–1021, Jul. 2009, doi: 10.1007/s00586-009-0936-6.

[7] S. T. Dukkipati and M. Driscoll, "Development and biomechanical evaluation of a 3D printed analogue of the human lumbar spine," *3D Printing in Medicine 2025 11:1*, vol. 11, no. 1, pp. 1–9, Jan. 2025, doi: 10.1186/S41205-025-00249-Y.

[8] S. T. Dukkipati and M. Driscoll, "Design Improvements and Validation of a Novel Fully 3D Printed Analogue Lumbar Spine Motion Segment," *J Bionic Eng*, vol. 21, no. 3, pp. 1388–1396, May 2024, doi: 10.1007/s42235-024-00512-8.

[9] P. W. Hodges *et al.*, "In vivo measurement of the effect of intra-abdominal pressure on the human spine," *J Biomech*, vol. 34, no. 3, pp. 347–353, Mar. 2001, doi: 10.1016/S0021-9290(00)00206-2.

[10] K. Daggfeldt and A. Thorstensson, "The role of intra-abdominal pressure in spinal unloading," *J Biomech*, vol. 30, no. 11–12, pp. 1149–1155, Nov. 1997, doi: 10.1016/S0021-9290(97)00096-1.

[11] T. K. Rupp *et al.*, "A forward dynamics simulation of human lumbar spine flexion predicting the load sharing of intervertebral discs, ligaments, and muscles," *Biomech Model Mechanobiol*, vol. 14, no. 5, pp. 1081–1105, Oct. 2015, doi: 10.1007/s10237-015-0656-2.